Mine Water Environ (2011) 30:2–21
DOI 10.1007/s10230-010-0127-z

TECHNICAL ARTICLE

Predicting Geochemical Behaviour of Waste Rock with Low Acid Generating Potential Using Laboratory Kinetic Tests

B. Plante · M. Benzaazoua · B. Bussière

Received: 25 February 2010 / Accepted: 24 September 2010 / Published online: 9 October 2010

Abstract Prediction of contaminated neutral drainage using laboratory kinetic tests designed for acid mine drainage prediction is challenging because of the low metal concentrations generated by low sulfide oxidation rates. Fresh and weathered samples from the Tio mine waste rock piles were submitted to humidity cell tests. The waste rocks were demonstrated to be non-acid generating in the long term, as interpreted by conservative oxidation-neutralization curves. The results demonstrate that even though the main neutralizing minerals react differently after 25 years of natural weathering (with regard to Ca, Mg, Al, and Si release), the response of the fresh waste rocks during humidity cell leaching was very similar to those of the weathered waste rocks, when considering all the elements related to silicate dissolution, including those implicated in secondary phase precipitation. However, Ni generation was greater in the weathered waste rocks even though sulfide oxidation rates were similar, as Ni sorption properties reach saturation. Although the Ni concentrations from the leachates of humidity cell tests remain below regulated values, they are bound to increase with continued weathering if no preventive or control measures are undertaken at the site.

Keywords Contaminated neutral drainage · Humidity cell tests · Nickel · Tio mine waste rocks · Weathering

Electronic supplementary material The online version of this article (doi:10.1007/s10230-010-0127-z) contains supplementary material, which is available to authorized users.

B. Plante (✉) · M. Benzaazoua · B. Bussière
Univ du Québec en Abitibi-Témiscamingue (UQAT), 445 boul de l'Université, Rouyn-Noranda J9X 5E4, QC, Canada
e-mail: benoit.plante@uqat.ca

B. Plante · M. Benzaazoua · B. Bussière
Industrial NSERC-Polytechnique-UQAT Chair in Environment and Mine Waste Management, UQAT, Rouyn-Noranda, QC, Canada

M. Benzaazoua
Canada Research Chair on Integrated Management of Mine Waste, UQAT, Rouyn-Noranda, QC, Canada

B. Bussière
Canada Research Chair on the Restoration of Abandoned Mine Sites, UQAT, Rouyn-Noranda, QC, Canada

Introduction

The remediation costs of mine waste that generates acid mine drainage (AMD) are about 10 times that of non-acid-generating wastes (Aubertin et al. 2002; Bussière 2007); therefore, accurate AMD prediction is crucial for an integrated mine waste management and proper remediation of mine sites. However, many toxic metals, such as Ni, Zn, Co, As, and Sb, are soluble at near-neutral pH, and can potentially contaminate mine effluents, even without acidic conditions; this phenomenon is called contaminated neutral drainage (CND) or simply neutral drainage (Bussière 2007; Heikkinen et al. 2009; Nicholson 2004; Pettit et al. 1999). CND occurs when sufficient neutralization is available in the mine wastes and/or when sulfide oxidation is sufficiently weak (Heikkinen et al. 2009). Prediction techniques developed for AMD generation prediction (Blowes et al. 2003; Lawrence and Scheske 1997; Lawrence and Wang 1997; MEND 1991; Paktunc 1999b; White et al. 1999) might not be suitable for CND generating sites (Nicholson 2004). Li (2000) demonstrated that for low-sulfide, low-neutralization potential mine wastes, the proportion of dissolved carbonates that effectively neutralize acid

decreases when sulfide oxidation drops below a certain rate, because the bicarbonate ions are dissolved and flushed out of the material without acid neutralization.

Many cases can be found in the literature where Ni CND is generated from tailings with significant carbonate neutralization and various sulfide oxidation levels (Heikkinen and Räisänen 2008; Heikkinen et al. 2009). It was also demonstrated (Li 2000) that the silicate contribution to neutralization becomes increasingly important as sulfide oxidation rates drop. Many studies are found in the literature where the unoxidized portion of AMD generating tailings show CND-like features such as near-neutral pH and high dissolved nickel levels (e.g. Gunsinger et al. 2006; Heikkinen and Räisänen 2008; Heikkinen et al. 2009; Holmström et al. 2001; Johnson et al. 2000; McGregor et al. 1998), where Ni levels are controlled mainly by sorption and/or coprecipitation with iron oxyhydroxides. However, no studies were found where Ni CND resulted from low sulfide oxidation with significant silicate neutralization. The present study focuses on water quality prediction of Ni CND generating mine waste rocks by means of kinetic tests, at a site where acid neutralization is mainly provided by silicate minerals. The tests were performed on waste rocks sampled from the Tio mine, a hematite-ilmenite deposit near Havre-Saint-Pierre, Québec, Canada (Fig. 1), exploited since the early 1950's through an open pit operation by Rio Tinto, Iron and Titanium Inc. The gangue material of the Tio ore is mainly composed of a calcic plagioclase mineral close to labradorite composition (approximate formulae $Na_{0.4}Ca_{0.6}Al_{1.6}Si_{2.4}O_8$; see Pepin 2009; Plante et al. 2010a). The gangue also contains pyroxene, chlorite, mica and biotite. Effluents from the waste rock piles are near-neutral and sporadically show Ni concentrations slightly higher than those allowed by applicable local regulations (QIT 2005). Preliminary studies performed on a concentrated sulfides fraction of the Tio mine waste rocks, prepared from froth flotation, showed that Ni is generated mainly from Ni-bearing pyrite (FeS_2) and millerite (NiS) that seem to be associated with ilmenite in the Tio ore deposit (Bussiere et al. 2005). Other sulfide oxidation products include Co and Zn. A Tio mine waste rock sample previously studied was shown to be non-acid-generating (Bussiere et al. 2005). The work also demonstrated that the waste has important metal retention potential, occurring most probably via surface sorption (Bussiere et al. 2005; Pepin et al. 2008; Plante et al. 2008; Plante 2010).

Literature Background

The two main gangue minerals found in the Tio mine waste rocks are plagioclases and pyroxenes (Plante et al. 2010a), and the waste rocks can contain up to approximately 70–80% residual ilmenite ore. The dissolution mechanisms of these minerals and the formation of layered double hydroxides, which are believed to play an important role in the metal uptake of silicates, are reviewed below.

Plagioclase Reactivity

The plagioclases are a solid solution series within the feldspar mineralogical family. The series range from albite to anorthite end-members with respective compositions of $NaAlSi_3O_8$ and $CaAl_2Si_2O_8$, where sodium and calcium atoms can substitute for each other in the mineral's crystal lattice structure. Plagioclase dissolution have been long known to be incongruent, with Al, Na and Ca being preferably dissolved at the surface (e.g. Blum and Stillings 1995; Carroll and Knauss 2005; Casey et al. 1989; Inskeep et al. 1991; Muir et al. 1989, 1990a, b; Schweda et al. 1997). This dissolution generates an Al–Na-Ca-poor thin layer (which is consequently enriched in Si) at the plagioclase surface (Blum and Stillings 1995). The formation of silica enriched residual layers on feldspars in acidic solution is a multi-step process. First, the exchange of Na^+ and Ca^{2+} for H^+ (Blum and Stillings 1995; Muir and Nesbitt 1997; Muir et al. 1990a, b; Scheweda et al. 1997) results in an increase in solution pH (Blum and Stillings 1995). Second, Al^{3+} is preferentially released into solution due to the breaking of Si–O–Al bonds preferentially over Si-0-Si bonds (Muir and Nesbitt 1992, 1997; Muir et al. 1990a, b; Xiao and Lasaga 1994), which is also an acid-consuming step (Muir et al. 1990a, b). The second reaction step implies that Al is preferentially released from the plagioclase into solution, after which Si is released (Muir and Nesbitt 1997). A third step is also suggested for feldspar dissolution, which implies repolymerization of Si–O bonds, releasing acid into solution (Muir et al. 1990a, b; Schweda et al. 1997). Since labradorite (the plagioclase in the Tio waste rocks, see Table 3) is net-neutralizing (Jambor et al. 2007), the overall reaction must be acid-consuming; therefore, the third reaction step must release less acid than was consumed in the first two reaction steps.

According to Blake and Walter (1999), the thickness and composition of leached layers on feldspars depends on solution composition and pH. Dilute acidic conditions produce relatively thick Si-rich layers, up to several thousands of Å (e.g. Blum and Stillings 1995; Casey et al. 1989; Hellmann et al. 2003; Muir and Nesbitt 1992, 1997), whereas dissolution at near-neutral pH produces only thin leached layers of tens of Å between pH 5 and 8 (Blake and Walter 1999; Blum and Stillings 1995; Muir and Nesbitt 1997). The circumneutral environments prevailing in the Tio mine waste rock kinetic tests should promote the formation of such thin leached layers (tens of Å) on the plagioclase feldspar surfaces.

Fig. 1 Geographic location of the Tio mine site

The Al released from labradorite dissolution could precipitate as various possible secondary phases, such as kaolinite ($Al_2Si_2O_5(OH)_4$) or $Al(OH)_3$, as demonstrated by geochemical simulations with VMinteq and JCHESS (Figs. 7, 8 respectively). The labradorite reaction with acid leading to kaolinite precipitation can be generalized and simplified as Eq. 1, while the same reaction leading to aluminum hydroxide is generalized as Eq. 2:

$$Ca_{0.6}Na_{0.4}Al_{1.6}Si_{2.4}O_8 + 1.6H^+ + 2.4H_2O \rightarrow 0.8Al_2Si_2O_5(OH)_4 + 0.8H_4SiO_4 + 0.4Na^+ + 0.6Ca^{2+} \quad (1)$$

$$Ca_{0.6}Na_{0.4}Al_{1.6}Si_{2.4}O_8 + 1.6H^+ + 6.4H_2O \rightarrow 1.6Al(OH)_3 + 2.4H_4SiO_4 + 0.4Na^+ + 0.6Ca^{2+} \quad (2)$$

Pyroxene Reactivity

The pyroxenes found in the Tio mine waste rocks are represented mainly by enstatite (6.1–24.9 wt%) in Table 3. Enstatite neutralizes acid through Eq. 3 (Oelkers and Schott 2001; Stefánsson 2001):

$$MgSiO_3 + 2H^+ + H_2O \rightarrow Mg^{2+} + H_4SiO_4 \quad (3)$$

Enstatite dissolution proceeds via magnesium releasing exchange reactions between aqueous H^+ and Mg^{2+} in the enstatite structure, followed by the relatively slow detachment of silica from partially liberated tetrahedral chains (Oelkers and Schott 2001; Oelkers et al. 2009; Zakaznova-Herzog et al. 2008). Enstatite is believed to exchange about 3.1 hydrogen atoms for each Mg at the reacting sites, following Eq. 4:

$$MgSiO_3 + 3.1H^+ \rightarrow H_{3.1}SiO_3^{1.1} + Mg^{2+} \quad (4)$$

Thus, pyroxenes preferentially release Mg over Si in early dissolution stages, much like the plagioclases preferentially release Ca and Na over Si initially. The preferential release of Mg from pyroxene is expected to lead to the formation of Mg-depleted/Si- and H-enriched surfaces. From XPS (X-ray photoelectron spectroscopy) results of enstatite leached at pH 6, model calculations indicate an Mg-depleted weathered surface layer of only a few atoms thick, while continuous leaching near pH 1 and at elevated temperatures (up to 60°C) leads to formation of a weathered layer of pure silica (Schott et al. 1981).

Ilmenite Reactivity

Ilmenite ($FeTiO_3$) minerals may contain many substitutes within its crystal structure, most notably Mg and Mn (e.g. Lener 1997, and references therein). Ilmenite dissolution is known to be associated with Mg and Mn release (e.g. Grey et al. 2005; Hodgkinson et al. 2008; Nair et al. 2009; Schroeder et al. 2002); during ilmenite dissolution, Mg and Mn removal is believed to follow Fe release (Lener 1997). In the case of naturally weathered ilmenite, Grey and Reid (1975) proposed a two-stage alteration mechanism, which is currently the generally accepted model (Janßen et al. 2008). In the first stage, ilmenite undergoes weathering through oxidation and removal of Fe to form a transitional phase consisting of an apparently continuous series of compositions from ilmenite to pseudorutile (ideally $Fe_2Ti_3O_9$) (Eq. 5):

$$FeTiO_3 + 2H^+ + {}^1\!/_2O_2 \rightarrow Fe_2Ti_3O_9 + Fe^{2+} + H_2O \quad (5)$$

The Fe is assumed to diffuse out through the unaltered oxygen lattice. In the second stage, pseudorutile undergoes incongruent dissolution (Eq. 6), resulting in the formation of rutile (TiO_2) and/or leucoxene (Frost et al. 1983; Nair et al. 2009), which is believed to be the ultimate alteration product of ilmenite (Lener 1997; Nair et al. 2009; Schroeder et al. 2002):

$$Fe_2Ti_3O_9 + 4H^+ \rightarrow 3TiO_2 + 2Fe^{2+} + 2H_2O + {}^1\!/_2O_2 \quad (6)$$

It was also proposed (White and Peterson 1996; White et al. 1994) that ilmenite could dissolve in anoxic conditions at pH 1–7 following Eq. 7:

$$FeTiO_3 + 2H^+ \rightarrow TiO_2 + Fe^{2+} + H_2O \quad (7)$$

Ilmenite dissolution is a neutral process (it neither consumes nor produces acid) at near-neutral/oxic conditions such as those encountered in the present study, because the oxidation and hydrolysis of each ferrous ion released by ilmenite dissolution will produce $2H^+$ (Eqs. 8 and 9), which are equivalent to the H^+ consumed by each ilmenite or pseudorutile while dissolving:

$$Fe^{2+} + {}^1\!/_4O_2 + H^+ \rightarrow Fe^{3+} + {}^1\!/_2H_2O \quad (8)$$

$$Fe^{3+} + 3H_2O \rightarrow Fe(OH)_3 + 3H^+ \quad (9)$$

Layered Double Hydroxides (LDH)

Metal uptake by mineral surfaces may be attributed to a number of different processes. Sparks (2001, and references therein) indicates that sorption of metals such as Ni and Co on soils results in the formation of metal hydroxide precipitate phases. In the case of Al-bearing soil mineral sorbents, the precipitates are metal-Al hydroxides called layered double hydroxides (LDH) (e.g. d'Espinose de la Caillerie et al. 1995; Eick et al. 2001; Roberts et al. 1999; Scheidegger et al. 1997, 1998; Scheinost and Sparks 2000; Scheinost et al. 1999; Sparks 2001; Yamaguchi et al. 2002).

These superficial precipitates occur at metal releases far below theoretical monolayer coverage, in a pH-range well below that where the precipitation of metal hydroxides would be expected based on thermodynamic solubility, and at time scales as fast as 15 min (Scheidegger et al. 1998; Sparks 2001). It was established that such LDH phases preferentially form in the presence of Al-containing sorbents like kaolinite, gibbsite, and alumina above pH 7.0 (Scheinost and Sparks 2000). Ni–Al LDH was established to form on gibbsite of low-surface area over pH 7.5, while on high-surface area gibbsite, Ni was sorbed as an inner-sphere complex (Yamaguchi et al. 2002). It was also shown to form on a soil clay fraction (composed of aluminum hydroxy interlayered vermiculite, kaolinite, mica with minor amounts of gibbsite and quartz) at pH 7.5 (Roberts et al. 1999), less so at pH 6.8, but not at pH 6.0. Moreover, Ni sorption rates significantly increased with pH. It was also demonstrated that LDH were thermodynamically and/or kinetically favored rather than the formation of hydroxides when an Al-releasing sorbent is available at near-neutral pH (Scheinost et al. 1999; Peltier et al. 2006).

It was also demonstrated that Ni–Al LDH become increasingly stable as they age and that over time, these precipitates will transform into more stable Ni-phyllosilicates (Ford et al. 1999; Peltier et al. 2006; Roberts et al. 1999; Scheckel and Sparks 2001; Scheckel et al. 2000).

Materials and Methods

Characterization Methods

The specific gravity (Gs) of the waste rock samples was determined with a Micromeritics helium pycnometer. The specific surface area (S.S.A.) was determined by using a Micromeritics surface area analyzer using the B.E.T method (Brunauer et al. 1938). The grain size distribution was determined by sieving for the fractions between 10 cm and 0.355 μm and by a laser diffraction grain size analyzer for the <0.355 μm fraction using a Malvern Instruments Mastersizer S. The Tio mine waste rock chemical analysis was performed using acid digestion (HNO_3-Br_2-HF-HCl) followed by ICP-AES analysis for over 20 elements. Silica is partially evaporated during the digestion procedure and therefore is not reported in this study. Sulfide sulfur was determined by subtracting the sulfate sulfur (determined by a 40% HCl extraction; method adapted from Sobek et al. 1978) from the total sulfur (ICP-AES analysis). The waste rock samples mineralogical characterization was performed with a Bruker A.X.S. D8 advance x-ray diffraction (XRD) instrument equipped with a copper anticathode. Mineralogical quantification was performed with Rietveld (1993) fitting of the XRD data with TOPAS software, with a detection limit and precision of approximately 0.1–0.5 wt%. Acid–base accounting (ABA) was determined following the protocol prescribed by Lawrence and Wang (1997). The acid-generation potential (AP) was calculated assuming that the sulfide sulfur content was exclusively expressed as pyrite and that all pyrite was available for oxidation, and converted to calcite equivalents (kg $CaCO_3$/t) by multiplying by a factor of 31.25. The neutralization potential (NP) was determined by HCl additions followed by back-titration of the excess acid to a pH 8.3 endpoint. The net neutralization potential (NNP) is the difference between the AP and NP (NNP = NP-AP), and the NP/AP ratio was also determined for interpretation purposes. Scanning electron microscope (SEM) observations of backscattered electrons (BSE) were made on a Hitachi S-3500 N microscope equipped with an x-ray energy dispersive spectrometer (EDS) analyzed with INCA software, at 20 kV and 100–130 μA. Oxygen was stoichiometrically determined by EDS analyses.

Kinetic Prediction Procedure

The geochemistry of the Tio mine waste rock was evaluated using humidity cell tests (ASTM D5744-96 2001), which consist of weekly drying-wetting cycles ending with flushing of the studied material (1 kg) with deionized water (1 L), and analysis for various geochemical parameters such as pH and metals concentrations in the leachates (using ICP-AES). These cell tests were performed for 76 cycles (539 days) on the <6.3 mm fraction of the mine wastes (believed to be the most reactive, e.g. Price and Kwong 1997) without grinding, since that would generate unwanted fresh surfaces in the weathered waste rock samples.

Geochemical Simulations

Geochemical speciation models are widely used to describe solid/water chemistry in mine drainage waters (e.g. Alpers and Nordstrom 1999; Blowes et al. 2003; Bussiere et al. 2004; Villeneuve et al. 2003). Such models calculate the ion activities and speciation over a wide range of conditions (such as temperature, pressure, concentration, pH, and Eh), and are used to calculate the saturation indexes of a wide variety of minerals and of the distribution of the elements between the aqueous, gaseous, and solid phases. Two different geochemical speciation models were used in this study: Visual Minteq (Felmy et al. 1984), which is a windows version of the MINTEQA2 ver.4.0 database (USEPA 1999), was employed for saturation index calculations, and; JCHESS (van der Lee and De Windt 2002), a graphical front-end of the CHESS model built from the EQ3/6 database (Wolery 1992), was employed for Eh–pH diagrams.

Samples Tested

Since the Tio mine has been in operation since the early 1950's, the waste rock piles have been submitted to natural weathering phenomena (up to over 5 decades at the time of sampling). Moreover, the waste rock composition varies significantly, as the target cut-off for ore processing is 76% hemo-ilmenite. Therefore, the hemo-ilmenite content of the waste rocks range between 0 and 76%. Also, the mine exploits two different ore bodies (Tio and Northwest) that have slightly different compositions (Plante et al. 2010a). The waste rock samples were carefully selected to represent the waste rock pile heterogeneity in terms of composition, origin, and age. Table 1 lists the general characteristics of the samples selected for the present study, as well as the ilmenite levels target during sampling (C1 < C2 < C3 for fresh and C4 < C5 < C6 for weathered

Table 1 Physical characteristics of the waste rock samples studied ($D_{x,}$ in µm, refers to the size for which x% of the sample is under this grain size)

	Age	Hemo-ilmenite (%)	Orebody	% <80 µm	D_{10}	D_{50}	D_{90}	C_u
C1	<1 month	20	Tio	7.1	163	1,285	4,310	10.7
C2	<1 month	40	Northwest	5.5	258	2,000	5,050	9.9
C3	<1 month	60	Northwest	4.7	320	1,900	4,590	7.4
C4	Approximately 25 year	20	Tio	6.7	174	1,270	4,380	10.1
C5	Approximately 25 year	40	Tio	8.6	114	1,200	4,820	14.9
C6	Approximately 25 year	60	Tio	10.4	73.0	1,305	4,860	26.0

samples). All samples were screened to <10 cm at the mine site.

Characterization Results

The physical characteristics of the Tio mine waste rock samples are summarized in Table 1. The weathered waste rock samples are generally finer than the fresh waste rock samples, as indicated by the D_{10} (C1–C3: 163–320 µm, C4–C6: 73–174 µm), D_{50} (C1–C3: 1,285–2,000 µm, C4–C6: 1,200–1,305 µm), D_{90} (C1–C3: 4,310–5,050 µm, C4–C6: 4,380–4,860 µm) and % <80 µm (C1–C3: 4.7–7.1%, C4–C6: 6.7–10.4%) values. The chemical element analyses most relevant for the purpose of this study are shown in Table 2. Fe (19.4–33.7 wt%) and Ti (9.84–17.6 wt%), associated mainly with ilmenite and hematite, follow the levels targeted in the sample preparation (C1 < C2 < C3 and C4 < C5 < C6). Since Al, Ca, and Mg are associated with gangue minerals, their levels follow the inverse of Fe and Ti and vary from 3.54 to 8.68 wt% for Al, from 1.45 to 3.65 wt% for Ca and from 1.12 to 3.14 wt% for Mg in the waste rock samples. Mg levels are generally higher in weathered samples (2.34–3.14 wt%) than in fresh ones (1.12–1.75 wt%). Ni (280–430 ppm), Co (240–450 ppm), Cu (80–170 ppm), Mn (52–90 ppm), and Sb (270–470 ppm) levels are generally correlated with Fe and Ti. $S_{sulfide}$ values are significantly higher in the fresh waste rocks than in the weathered ones, most probably because of weathering (sulfide oxidation). $S_{sulfide}$ values range between 0.335 and 0.466 wt% in the fresh waste rock samples and from 0.134 to 0.167 wt% in the weathered ones. It was previously demonstrated (Pepin 2009; Plante et al. 2010a) that Ni in the Tio mine waste rocks was mainly mineralogically associated with the ilmenite and sulfides.

The ABA of the Tio mine waste rock samples are also shown in Table 2. The AP values of the fresh waste rock samples (10.5–14.6 kg $CaCO_3$/t) are higher than those of the weathered ones (4.2–5.2 kg $CaCO_3$/t). The NP values range from 6.1 to 8.6 kg $CaCO_3$/t. Consequently, all the NNP values fall inside the uncertainty zone of the test (±20 kg $CaCO_3$/t) as defined by SRK (1989). NP/AP ratios range between 0.6 and 1.7 and classify as likely (when <1) or possibly (between 1 and 2) ARD generating according to the Price et al. (1997) criterion. However, the NP values are quite low and the uncertainty of the method (±2 kg $CaCO_3$/t, based on a 39 kg $CaCO_3$/t reference sample; Plante 2005) is quite high for the low NP values, leading to relative errors from 23 to 33%. Thus, ABA interpretation from such low values is difficult.

Table 2 Chemical and ABA characterization of the studied samples (elemental values in wt%, AP, NP, NNP in kg $CaCO_3$/t, NP/AP unitless)

	C1	C2	C3	C4	C5	C6
Al (wt%)	8.68	4.62	3.54	6.21	5.58	4.47
Ba (ppm)	220	170	130	190	160	140
Ca (wt%)	3.65	1.94	1.45	2.62	2.24	1.70
Co (ppm)	200	310	420	240	330	340
Cr (ppm)	200	320	540	460	550	630
Cu (ppm)	230	410	460	250	320	320
Fe (wt%)	19.4	27.8	33.7	23.6	27.0	30.9
Mg (wt%)	1.12	1.38	1.75	3.14	2.41	2.34
Mn (ppm)	350	540	740	730	750	790
Ni (ppm)	220	490	440	310	320	380
S_{total} (wt%)	0.384	0.345	0.472	0.142	0.164	0.172
$S_{sulphate}$ (wt%)	0.012	0.010	0.006	0.008	0.005	0.005
$S_{sulphide}$ (wt%)	0.372	0.335	0.466	0.134	0.159	0.167
Sb (ppm)	70	130	190	100	140	240
Ti (wt%)	9.84	14.1	17.6	10.4	12.8	14.9
Zn (ppm)	40	50	50	70	60	60
AP	11.6	10.5	14.6	4.2	5.0	5.2
NP	8.8	6.3	8.6	7.3	6.1	6.1
NNP	−2.8	−4.2	−6.0	3.1	1.1	0.9
NP/AP	0.8	0.6	0.6	1.7	1.2	1.2

The XRD quantification results are presented in Table 3. Pyrite is the main sulfide mineral detected (1.1–3.0 wt%), while chalcopyrite was detected at trace levels (0.1–0.6 wt%); no nickel sulfide was detected by XRD in the samples studied. The ore minerals ilmenite (23.0–45.2 wt%) and hematite (7.9–20.1 wt%), referred to as hemo-ilmenite since

they occur as exsolution lamellae in the Tio mine deposit, confirm the variation following the low, intermediate, and high ilmenite levels targeted in sample preparation (C1 < C2 < C3 and C4 < C5 < C6). The plagioclase mineral labradorite (main gangue mineral in the Tio deposit) levels are inversely proportional to the hemo-ilmenite content and ranges between 16.0 and 44.6 wt%. Other important gangue minerals in the Tio mine waste rock samples include the pyroxenes enstatite and pigeonite, with levels up to 24.7 and 3.7 wt% respectively. The micas biotite and muscovite (<3.1 wt%), chlorites (<3.3 wt%), K-felsdpar orthoclase (up to 6.8 wt%), rutile (<2.0 wt%), and spinel (up to 6.5 wt%) complete the Tio mine waste rock samples mineralogy.

Results and Interpretation

Humidity Cells

As shown in Table 3, no carbonate mineral was detected in the Tio mine waste rocks. Consequently, neutralization of the acid resulting from sulfide oxidation is provided mainly by silicate minerals, particularly by the calcic plagioclase mineral (identified as labradorite in the XRD analyses) and the pyroxenes (enstatite and pigeonite), and possibly also from the minor gangue minerals phlogopite mica (biotite) and chlorite, based on the classification of silicate dissolution in static ABA testing (Jambor et al. 2007). The dissolution products considered in the present study that come from the neutralizing processes are Ca, Al, Mg, and Si. According to the classification of the relative mineral reactivities at pH 5 of Kwong (1993), pyroxenes react faster than plagioclases. However, the Jambor et al. (2002, 2007) NP comparisons on pure minerals showed that the plagioclase mineral labradorite neutralizes more acid than pyroxenes.

The humidity cell tests results are shown in Figs. 2 and 3. The pH of all the cell leachates remained near-neutral over 529 testing days. The weathered waste rocks generally generate leachates with lower pH values (6.5–8) than the fresh waste rocks (7.5–9.0) during the first 150 days, after which no significant differences were observed (pH between 6.5 and 8.5). The electric conductivities of the leachates stabilized rapidly between 10 and 100 µS/cm, and remained so until the last leaching cycle. Leachate Ca concentrations stabilized after approximately 50 days; the weathered waste rocks cells generated lower Ca levels (1–2 mg/L) than the fresh ones (2–10 mg/L). The Al concentrations from the fresh waste rock cells diminished from the beginning of the test until approximately 400 days, after which they increased until the end of the test. Al concentrations generated from the weathered samples remained very close to or below the analytical detection limit (0.01 mg/L) throughout the tests. The weathered waste rock cells generated higher Mg and Si levels than fresh ones (Mg: up to 0.13 mg/L for C1–C3 and up to 0.61 mg/L for C4–C6; Si: <5 mg/L for C1–C3 and up to 22 mg/L for C4–C6). No significant differences between S (sulfates) values were noticed between the fresh and weathered waste rocks (0.3–1.1 mg/L). The Ni values were generally less than the detection limit (0.004 mg/L) for the fresh waste rock leachates and the C5 sample. The Ni loadings of the C4 and C6 weathered waste rock leachates stabilized between 0.005 and 0.010 mg/L after the first 130 days. Co and Zn levels were generally close to

Table 3 Mineralogical characterization of the kinetic and weathering cells materials by XRD and Rietveld quantification

Mineral	Formulae	C1	C2	C3	C4	C5	C6
Labradorite	$(Ca,Na)\ (Si,Al)_4O_8$	44.6	19.1	16.0	32.2	31.3	20.3
Ilménite	$FeTiO_3$	23.0	37.0	45.2	23.2	26.9	41.2
Hématite	Fe_2O_3	8.1	9.3	20.1	7.9	8.6	16.5
Pyrite	FeS_2	1.3	3.0	1.6	1.1	1.3	1.7
Chalcopyrite	$CuFeS_2$	0.5	0.5	0.2	0.4	0.6	0.1
Enstatite	$Mg_2Si_2O_6$	6.1	12.9	8.5	24.7	20.4	13.9
Pigeonite	$(Mg,Fe^{2+},Ca)\ (Mg,Fe^{2+})Si_2O_6$	3.7	3.2	0.5	2.1	2.8	2.2
Biotite	$K(Mg,Fe^{2+})_3\ (Al,Fe^{3+})Si_3O_{10}(OH,F)_2$	1.6	1.7	0.4	1.0	1.1	1.0
Muscovite	$KAl_2\ (Si_3Al)O_{10}(OH,F)_2$	0.1	1.1	0.5	1.2	0.7	0.0
Chlorite	$(Mg,Fe,Al)_6(Si,Al)_4O_{10}(OH)_8$	2.8	2.9	0.9	3.3	3.1	0.0
Orthoclase	$KAlSi_3O_8$	6.8	0.6	4.5	1.2	0.5	0.9
Rutile (anatase)	TiO_2	1.0	1.5	0.6	1.0	1.9	0.9
Spinel	$MgAl_2O_4$	0.2	6.5	0.7	0.1	0.2	0.7
Total		99.8	99.2	99.4	99.4	99.1	99.4

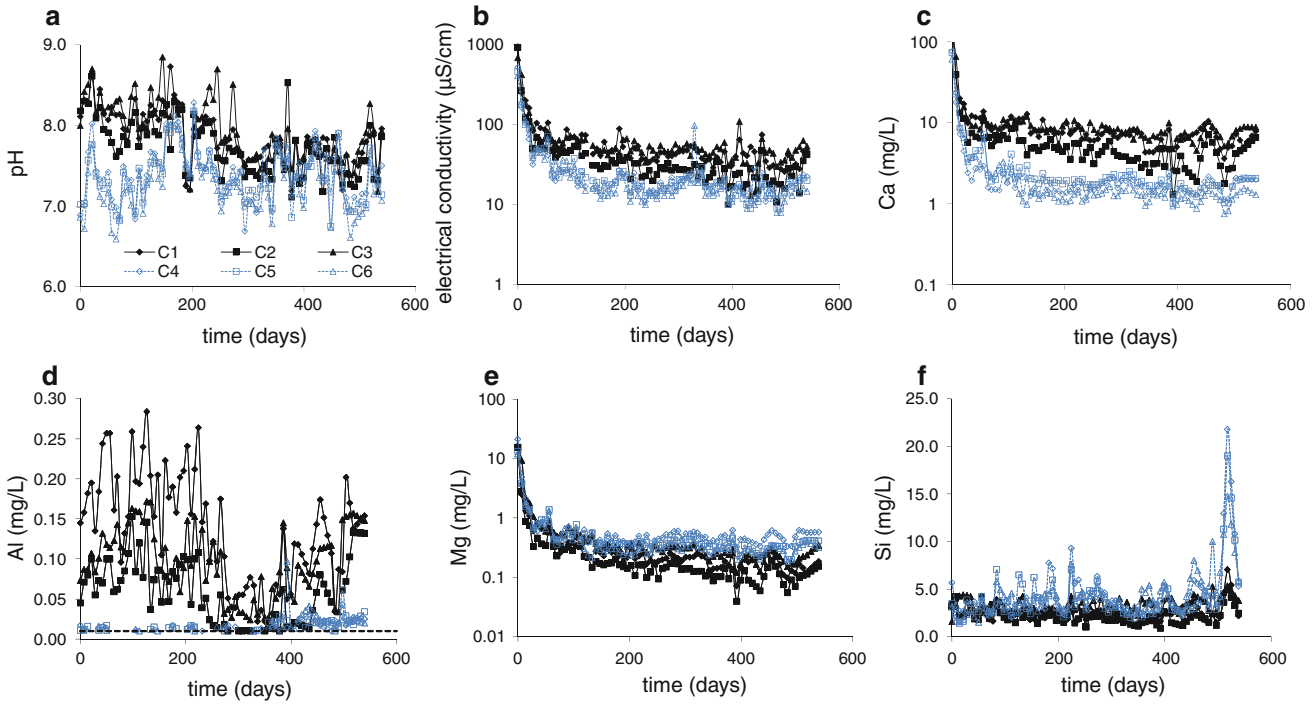

Fig. 2 Evolution of pH, conductivity, Ca, Al, Mg, and Si concentrations in humidity cell tests on Lac Tio waste rocks (note the log scale for conductivity, Ca, and Mg; *dashed lines* represent the ICP-AES detection limit)

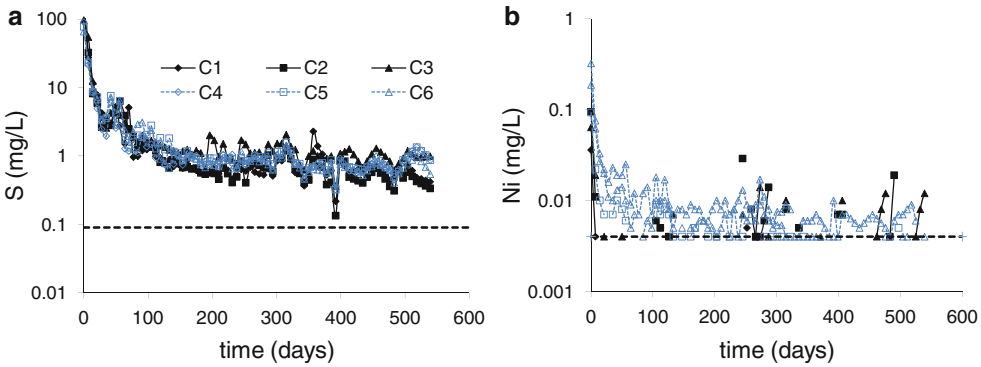

Fig. 3 Evolution of S and Ni concentrations from humidity cell tests (*dashed lines* represent the ICP-AES detection limit; results below the detection limit not shown)

the detection limit and are not relevant for the purpose of this study. Fe levels were below the detection limit most of the time in all cells; therefore, they are not shown.

Mineralogical Evolution During Tio Mine Waste Rock Weathering

The depletion curves for Ca (indicative of plagioclase dissolution) and S (as sulfates, indicative of sulfide oxidation) in humidity cells are shown in Fig. 4. The depletion curves show a first stage characterized by a rapid elemental decrease, followed by stabilization in a second stage, generally after 10–50 days. Such behavior was also observed by others (Benzaazoua et al. 2004; Cruz et al. 2001; Scharer et al. 1991, 1994). The rapid elemental depletions observed in the first depletion stage and the subsequent slowdowns are explained by at least three mechanisms: (1) dissolution of oxidation products and readily soluble phases, (2) fine particle disappearance due to complete dissolution and (3) surface passivation due to secondary minerals precipitation (Benzaazoua et al. 2004; Cruz et al. 2001; Scharer et al. 1991; Villeneuve et al. 2003). The Ca depletion slopes of the fresh samples are steeper than those of the weathered ones, while the S depletion slopes of the weathered samples are more similar to those of fresh ones. Ni depletions were negligible and are not reported in Fig. 4.

The evolution of the cumulative normalized loadings (mg/kg) in the flushed waters shown in Fig. 5 enable the determination of the elemental release rates (presented in

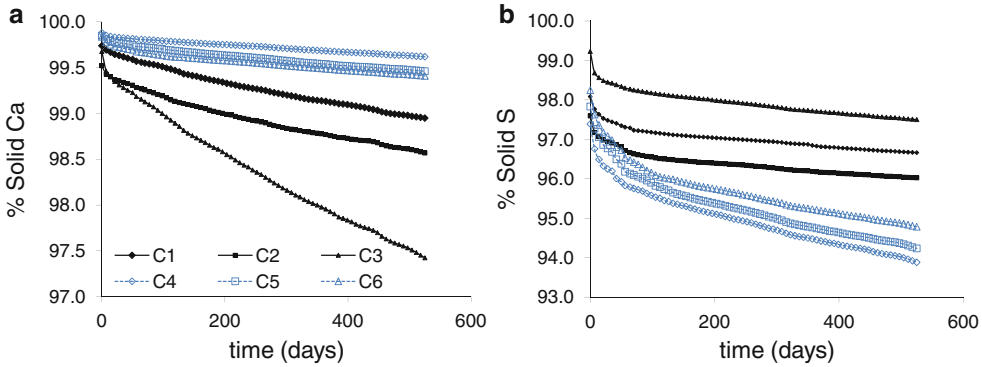

Fig. 4 Calcium (*left*) and sulfur (*right*) depletion curves for humidity cells

Table 4), by linear regression within the stabilized portion of the curves. It is important to point out the difference between the weathering rate and the release rate. According to Sapsford et al. (2009), the weathering rate is defined as the rate (mass per unit time, often normalized to unit mass or unit area) at which a primary mineral is transformed into secondary products, whether soluble or insoluble, congruently or incongruently, whereas the release rate is the rate at which an element or species is driven away from a unit mass of rock per unit time. In kinetic tests such as those used in the present study, the release rate is stoichiometrically related to the weathering rate of a given primary mineral only when the considered reaction products are entirely flushed (not retained in the material).

The applicability of the linear regressions used for the determination of the release rates are evaluated by the determination coefficients (R^2) shown in Table 4. Most R^2 values in Table 4 are close to unity ($R^2 \geq 0.97$), enabling interpretation and comparison of these release rates, especially for Ca, Mg, Si, and S. However, some R^2 values are farther from unity (R^2 as low as 0.37, Table 4), especially for elements with concentrations very close to the analytical detection limits in the leachates, like Al and Ni. The S release rates are similar for all samples studied and vary between 0.040 and 0.071 mg/kg/d (0.120 and 0.213 mg/kg/d as sulfates) in humidity cell tests. The S release rates obtained from the fresh and weathered waste rocks are of the same order. Assuming that all the sulfate ended up in the leachates, as no S-bearing oxidation products are suspected to form under the conditions of the kinetic tests (Online Supplementary Figures 1 and 2c), the S release rates are indicative of the sulfide weathering rates. The very low sulfate levels in the post-testing solids (≤30 ppm, not reported in this study; see Plante 2010) support this

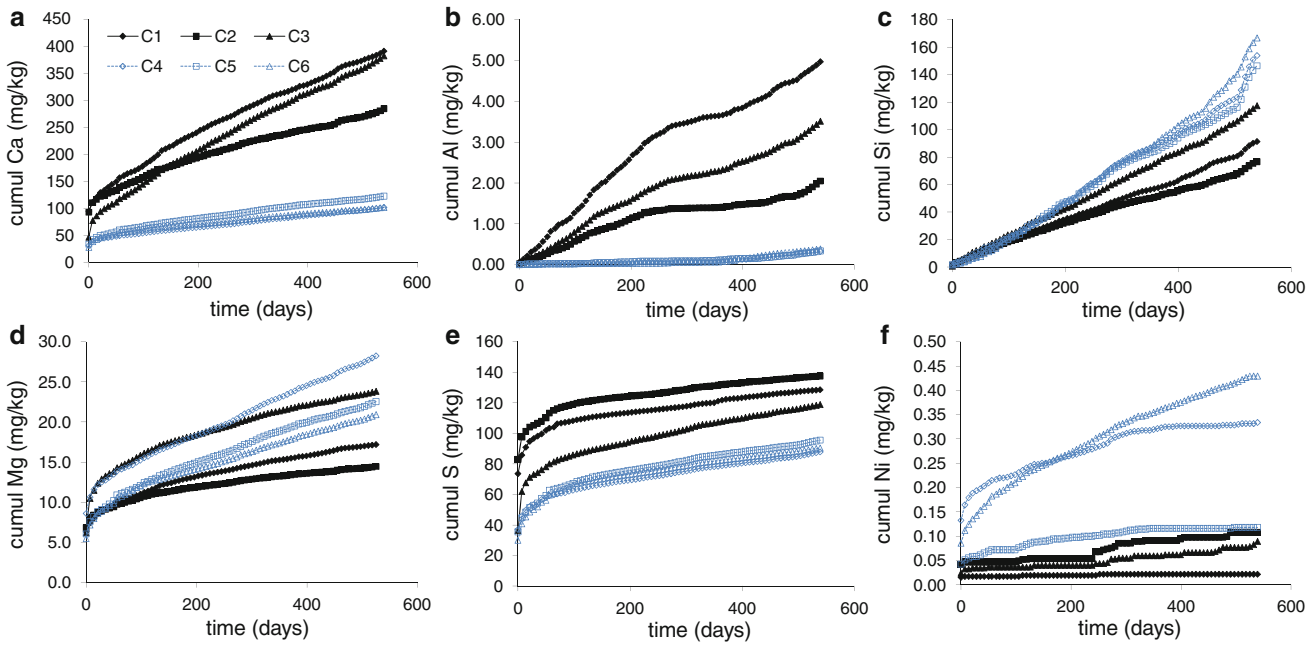

Fig. 5 Cumulative and normalized humidity cell loadings for oxidation/neutralization-related elements

Table 4 Elemental release rates and associated determination coefficients (R^2) from humidity and weathering cells tests (>200 days)

	Release rates (mg/kg/d)											
	Ca	R^2	S	R^2	Si	R^2	Mg	R^2	Al	R^2	Ni	R^2
C1	0.429	0.998	0.047	0.993	0.159	0.992	0.012	0.996	5.8E-03	0.974	4.7E-06	0.368
C2	0.245	0.995	0.040	0.988	0.119	0.991	0.008	0.991	1.8E-03	0.865	1.5E-04	0.860
C3	0.495	0.998	0.071	0.993	0.212	0.997	0.016	0.989	4.8E-03	0.972	1.2E-04	0.948
C4	0.108	0.999	0.052	0.995	0.267	0.969	0.031	0.998	7.2E-04	0.903	1.8E-04	0.792
C5	0.120	0.994	0.056	0.992	0.246	0.967	0.023	0.994	6.8E-04	0.851	6.0E-05	0.772
C6	0.088	0.997	0.050	0.994	0.319	0.976	0.021	0.998	1.1E-03	0.893	4.5E-04	0.990

assumption. Consequently, sulfide oxidation appears to occur at similar rates in the fresh and weathered waste rock samples when submitted to humidity cells.

The Ca release rates were significantly higher in the fresh waste rocks samples (0.245–0.495 mg/kg/d) than in the weathered ones (0.088–0.120 mg/kg/d), as expected from the previously explained plagioclase reaction mechanism (preferential Ca release form plagioclase in early weathering stage). Since no secondary Ca minerals should have precipitated, according to the thermodynamic simulations (Online Supplementary Figures 1 and 2), the Ca leached from the plagioclase is expected to have remained in solution during the kinetic tests. Consequently, the Ca release rates in the fresh waste rock samples are expected to be stoichiometrically related to the plagioclase weathering rate.

In the fresh waste rock samples, the Al release rates decreased at approximately 250 days, while the Si release rates increased after 400–450 days. The kinetic tests gave higher Si release rates in weathered samples, which suggest that weathered plagioclase surfaces in the Tio mine waste rock samples are already Ca and Al depleted, in accordance with the first two plagioclase reaction steps previously mentioned. As demonstrated in Online Supplementary Figure 1, there is only a slight difference in the Saturation Index values of the Si-bearing secondary minerals (kaolinite, imagolite, halloysite) between fresh and weathered waste rock samples. Therefore, secondary mineral precipitation in fresh waste rocks doesn't seem to be the main reason explaining the higher Si release rates in weathered samples. The higher Si release rates and lower Ca release rates in weathered waste rocks are consistent with the development of a Ca-poor, Si-rich layer over the weathered plagioclase surface; once the Ca is leached from the surface layer of the plagioclase, more Si is released into solution, as expected from the plagioclase reaction steps previously discussed. The third plagioclase dissolution step (Muir et al. 1990a, b; Schweda et al. 1997) is believed to release some of the acid adsorbed in the first two steps. The generally lower pH values obtained in the leachates obtained from weathered samples in humidity cell tests support this mechanism.

The Mg release rates, related mostly to pyroxene dissolution but also probably to ilmenite in lesser amounts since ilmenite releases Mg during its dissolution (e.g. Grey et al. 2005; Hodgkinson et al. 2008; Nair et al. 2009; Schroeder et al. 2002), were higher in weathered waste rocks (0.021–0.031 mg/kg/d) than in fresh ones (0.008–0.016 mg/kg/d), suggesting that pyroxenes and/or ilmenite seem to dissolve faster in weathered waste rocks. However, it is impossible from these results to specifically distinguish the behaviors of ilmenite and pyroxene. SEM images of altered ilmenite grains from the weathered sample C6 are shown in Fig. 6. Ilmenite grains in Fig. 6a, b, and d show obvious weathering of ilmenite preferentially over hematite. The EDS analyses of the weathered ilmenite shows almost complete Fe depletion, suggesting the remaining phase is something between pseudo-rutile (ideally, $Fe_2Ti_3O_9$) and leucoxene (believed to be similar to rutile, TiO_2). On every altered ilmenite grain observed from the present study, there are clear boundaries between the altered and primary ilmenite, which has also been observed in other studies (Mücke and Bhadra Chaudhuri 1991; Nair et al. 2006, 2009). Each ilmenite grain in Fig. 6 bears alteration products on the surface, even the apparently unaltered ilmenite grain shown in Fig. 6c; EDS analyses suggest that these secondary phases are mainly composed of Si, Al, and Mg. Moreover, thermodynamic simulations with JCHESS (Online Supplementary Figure 2b) suggests Mg-montmorillonite ($(Na,Ca)_{0.33}(Al,Mg)_2Si_4O_{10}(OH)_2{\cdot}nH_2O$) precipitation in the typical conditions encountered in the humidity cell tests in this study. More insight is needed to understand the nature of this secondary phase. This mineral is not included in the VMinteq database used in the thermodynamic simulations, which explains its absence in the possible secondary phases considered in Online Supplementary Figure 1. Finally, the Ni concentrations in the drainage waters are often below the analytical detection limit. Therefore, the rates had poor R^2 values (0.37–0.86) for most of the waste rock samples; only the C3 and C6 samples had high R^2 values (>0.95). It is therefore hazardous to link the Ni release rates to any mineralogical weathering rate in the present study.

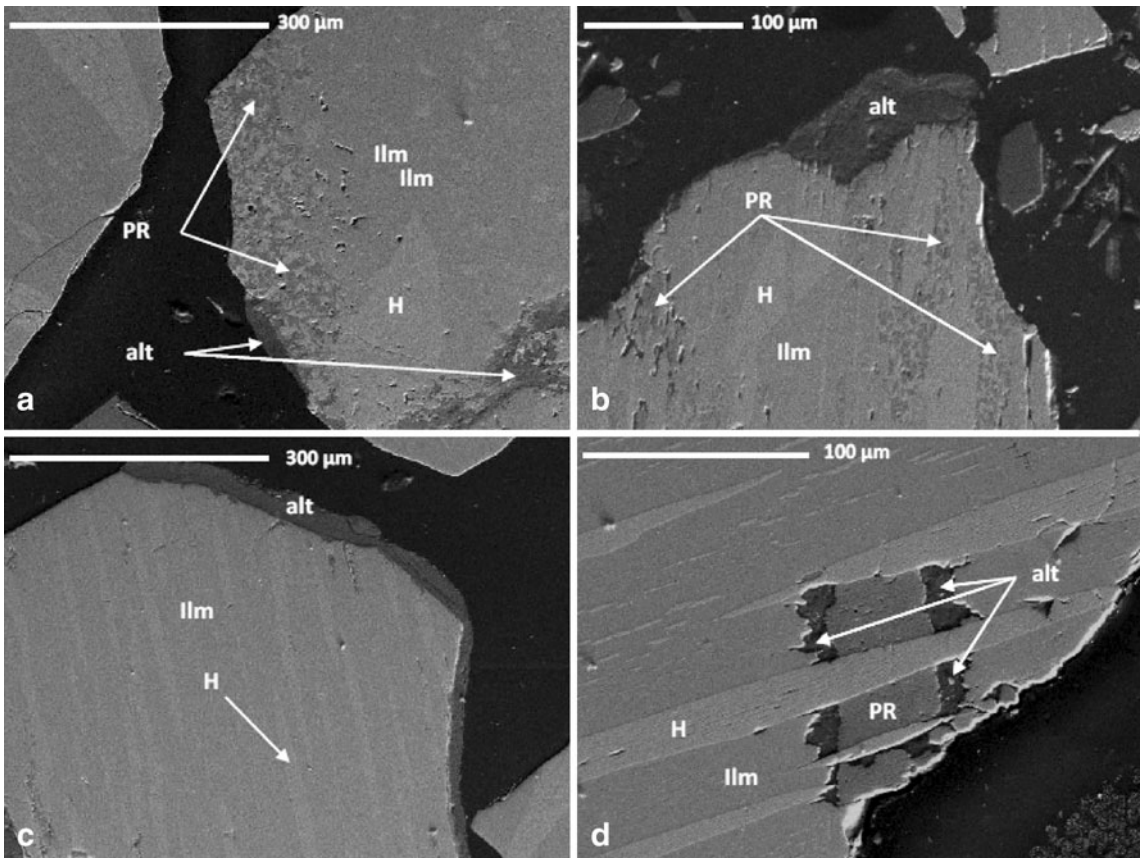

Fig. 6 SEM (BSE mode) images of altered hemo-ilmenite grains (Alt: Si, Al, Mg secondary phase; H: hematite; Ilm: ilmenite; PR: pseudorutile-like phase)

The differences in plagioclase weathering levels between samples are illustrated by plotting the cumulative normalized loadings of Ca vs. Si, and Al vs. Si, in Fig. 7a and b, respectively. It can be seen that the slopes of the Ca and Al vs. Si loadings from the fresh waste rocks tend to decrease over time. However, the slopes corresponding to the weathered waste rocks are significantly lower than those of fresh waste rocks. These tendencies show that weathering of the plagioclases within the fresh waste rocks in humidity cells have not reached the weathering level of the weathered waste rocks samples, even though there is a shift of the slopes from the fresh samples towards those of the weathered samples in Fig. 7a and b.

In the near-neutral conditions encountered in this study, Al could precipitate as various possible secondary phases like $Al(OH)_3$, kaolinite ($Al_2Si_2O_5(OH)_4$), or Mg-montmorillonite, as demonstrated by geochemical simulations with VMinteq and JCHESS (Online Supplementary Figures 1a, 1b and 2b). Consequently, Al precipitation as secondary minerals (such as kaolinite, Eq. 1) in the conditions of the kinetic tests could explain the low Al levels. No Al secondary minerals were detected by XRD, meaning that either these secondary minerals were present at less than the XRD detection limit (approximately 0.5 wt%) and/or that they are poorly crystallized and therefore undetectable by XRD. Poorly crystalline secondary minerals were established to form on weathered feldspar surfaces (Carroll and Knauss 2005; Casey et al. 1989; Hellmann et al. 2003; Nugent et al. 1998; Oberlin and Couty 1970; Zhang and Lüttge 2009, and references therein). The SEM images of weathered hemo-ilmenite grains (Fig. 6) also suggest that poorly crystallized secondary minerals containing Al, Mg, and Si were present. Another secondary mineral, which most probably precipitates in the Tio mine waste rocks, is illite $((K,H_3O)(Al,Mg,Fe)_2(Si,Al)_4O_{10}[(OH)_2,(H_2O)])$, although it was not detected in thermodynamic simulations (because K was not analyzed in the leachates and therefore not considered), nor by XRD. However, K is released by Tio waste rocks and illite minerals most probably precipitate, as demonstrated in another study on Tio waste rocks (Plante 2010). Moreover, K-bearing secondary minerals were observed in polished sections of waste rock samples from the present study (Plante et al. 2010b).

The higher Si release rates in weathered waste rocks may be partly attributable to the dissolution of poorly crystallized amorphous Si-bearing secondary minerals that

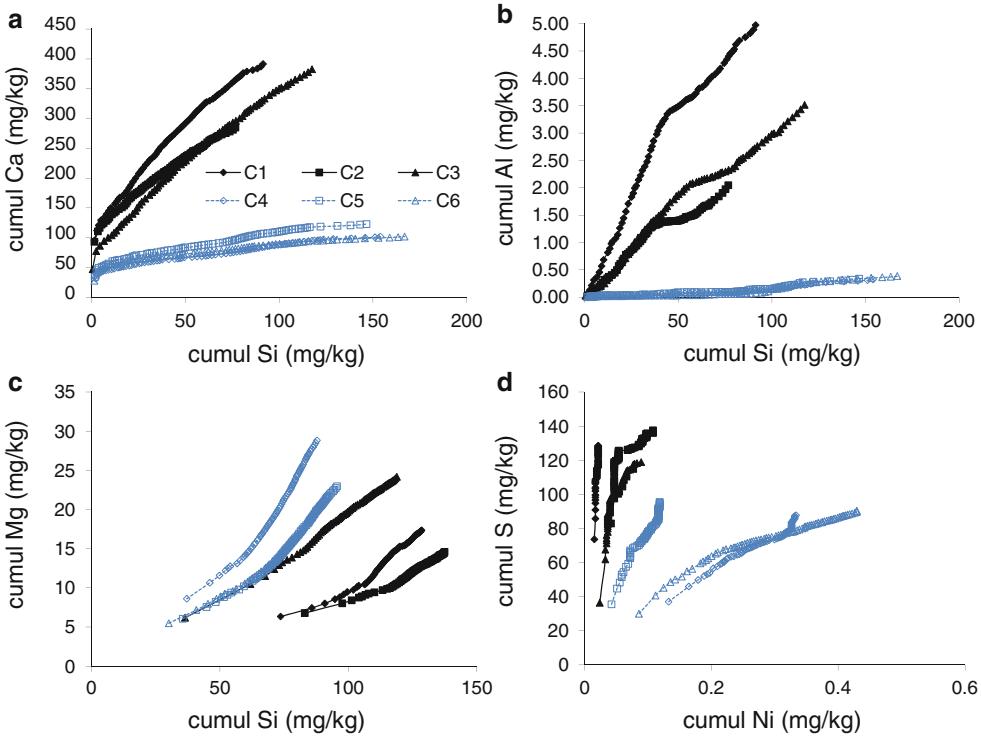

Fig. 7 Comparison of Ca–Si, Al–Si, and S-Ni cumulative values in humidity cells

could have formed on the surfaces either in the field or during kinetic testing. To illustrate the dissolution of such secondary phases, Eqs. 10 to 12 depict kaolinite dissolution. According to Cama et al. (2002), kaolinite dissolution in acid is expressed by Eq. 10. In near-neutral conditions, each Al^{3+} ion produced is hydrolyzed to $Al(OH)_3$, generating $3H^+$ ions (Eq. 11). The combination of kaolinite dissolution and $Al(OH)_3$ precipitation can be expressed as a neutral process (Eq. 12), as it neither produces nor consumes acid at near-neutral conditions (with Al^{3+} hydrolysis).

$$Al_2Si_2O_5(OH)_4 + 6H^+ \rightarrow 2Al^{3+} + 2H_4SiO_4 + H_2O \quad (10)$$

$$Al^{3+} + 3H_2O \rightarrow Al(OH)_3 + 3H^+ \quad (11)$$

$$Al_2Si_2O_5(OH)_4 + 5H_2O \rightarrow 2Al(OH)_3 + 2H_4SiO_4 \quad (12)$$

Therefore, the dissolution of Si-bearing secondary minerals like kaolinite could partially explain the higher Si release rates in weathered waste rock samples, in addition to incongruent dissolution of weathered plagioclase surfaces releasing more Si into solution than fresh ones and the increase of pyroxene reactivity. Plagioclase samples ($Ab_{90}An_{10}$, which is 90% albite and 10% anorthite, containing low Ca levels) naturally weathered in slightly acidic soils (pH 4.9–5.6) showed a largely amorphous Al enriched and Na depleted coating, and the depleted feldspar surfaces beneath the coatings were Al and Na depleted (Nugent et al. 1998). It was also demonstrated (Nugent et al. 1998) that these coatings developed within the first few months of field weathering. Finally, the coatings were obvious by AFM (atomic force microscopy) and detectable by SIMS (secondary ion mass spectrometry) and XPS (x-ray photoelectron spectroscopy) techniques, but largely undetected by SEM. Thus, it is possible that the plagioclases in the weathered Tio mine waste rocks (and after weathering of fresh waste rocks in the kinetic tests) were coated by an amorphous Al-bearing coating undetected by SEM and XRD in the present study.

Long Term Assessment of AMD Generation

The main neutralizing minerals in the Tio mine waste rocks are plagioclase (labradorite; 16–45 wt% in Table 3) and pyroxenes (enstatite/pigeonite; 9–27 wt% total in Table 3). The pyroxenes are known to dissolve faster than labradorite by about an order of magnitude (Brantley et al. 2003; Kwong 1993; Wilson 2004). However, labradorite is believed to be twice as effective in acid neutralization as pyroxenes when compared in static tests (Paktunc 1999a; Jambor et al. 2002, 2007). Hence, the reaction of pyroxenes to acid production could be increased by plagioclase depletion. The higher Mg release rates in weathered waste rock samples than those observed for fresh ones suggest that the pyroxene contribution to acid neutralization increases in the weathered waste rock (considering that Mg release from ilmenite is the same or lower in weathered samples). Ilmenite release is known to be related to Mg and

Mn release (e.g. Schroeder et al. 2002; Grey et al. 2005; Hodgkinson et al. 2008; Nair et al. 2009); the low Mn values (not reported in this study) obtained in the leachates from all waste rock samples do not enable an efficient discrimination of pyroxene and ilmenite dissolution (the main Mg sources in the waste rocks).

The long term assessment of AMD generation potential of mine wastes can be done using oxidation-neutralization curves (Villeneuve et al. 2003; Benzaazoua et al. 2004; Villeneuve 2004). These curves compare the evolution of the products of sulfide oxidation (dissolved S as sulfates in the present work) with those of acid neutralization (such as Ca and Mg from plagioclases and pyroxenes in the present study). The long term assessment of AMD generation is performed by extrapolating the oxidation-neutralization curves and by plotting the initial solid sample values for comparison; if the points plot on the oxidation side of the extrapolation, the material is likely AMD generating in the long term. This interpretation is based on the interdependent hypotheses that the ratio between the oxidation and neutralizing products stays linear, and that mineralogy will not affect the linearity of the long-term relation (e.g. depletion of a mineral, precipitation of a new secondary phase). It was demonstrated that these hypotheses were respected for the long term weathering of high neutralization potential mine tailings, for which the neutralization was mainly provided by carbonates (Benzaazoua et al. 2004) and by silicates (Hakkou et al. 2008).

In the Tio mine waste rocks, the main neutralization product not suspected to be affected by secondary mineral precipitation is Ca; the Ca cumulative normalized loadings against S in humidity cell tests are shown in Fig. 8a. The curves show two phases separated by an inflection point: a lower slope value in the first days of testing followed by a steeper slope for the rest of the duration. Such an inflection point towards the neutralization products was observed in studies involving carbonate neutralization (Villeneuve et al. 2003; Villeneuve 2004), and is caused by (1) surface passivation of the sulfides and/or (2) an exaggeration of the leaching of neutralization products (Villeneuve et al. 2003; Villeneuve 2004). Mineral surface passivation is the decrease in reactivity following secondary mineral precipitation; such passivation was measured on weathered pyrite by cyclic voltammetry (Cruz et al. 2001; Villeneuve et al. 2003; Villeneuve 2004). The surface passivation of the sulfides could explain the curve shapes obtained for the cumulative normalized S loadings shown in Fig. 5e. Preferential Ca release is believed to take place on the fresh waste rocks samples but not in the weathered ones, because of the plagioclase dissolution behavior presented in the literature background. In fact, the slope difference before and after the inflection point is more pronounced in the fresh than in the weathered waste rock samples, suggesting that the inflection point is mainly due to preferential Ca leaching from the plagioclases in early weathering stages. The slope and R^2 values of the linear regressions of the cumulative Ca vs. S curves are presented in Table 5; the slopes of the fresh waste rock samples (6.4–10.0) are significantly higher than those of the weathered ones (1.65–2.06), with satisfactory R^2 values ranging between 0.991 and 0.999. These results are a consequence of the non-stoichiometric Ca release in early plagioclase weathering stages.

The extrapolation of the oxidation-neutralization curves and the points of the initial Ca and S values are plotted in Fig. 9. The C1 and C2 initial Ca values plot very close to the extrapolated curves, while for C3, they plot as acid-generating (Fig. 9a); therefore the long-term AMD generation potential of the fresh waste rocks is uncertain to acid-generating. On the other hand, the weathered waste rocks Ca and S initial values (Fig. 9b) plot far from the extrapolations on the neutralization side, demonstrating that the waste rocks should not generate AMD in the long term. The preferential Ca release in fresh waste rocks, because of the plagioclase dissolution mechanism, explains these results. However, the interpretation hypotheses of these oxidation-neutralization curves are not respected for

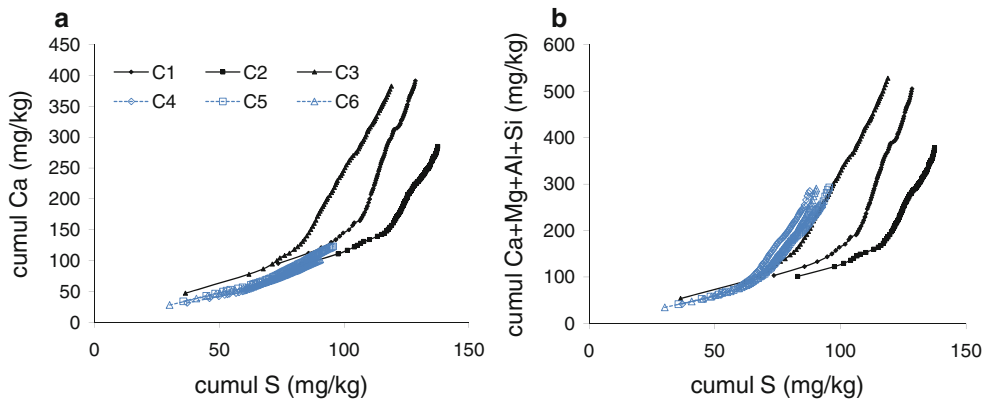

Fig. 8 Oxidation-neutralization curves for humidity cells considering Ca (**a**) and Ca + Mg + Al + Si (**b**) vs. S

Table 5 Characteristics of oxidation-neutralization curves for humidity cells (>70 days)

Waste rock sample	cumul. norm Ca/S		cumul. norm Ca + Mg + Al + Si/S	
	Slope	R^2	Slope	R^2
C1	10.0	0.991	13.8	0.993
C2	6.4	0.994	9.55	0.994
C3	7.0	0.999	10.0	0.998
C4	1.94	0.996	7.34	0.990
C5	2.06	0.998	6.51	0.990
C6	1.65	0.995	7.56	0.975

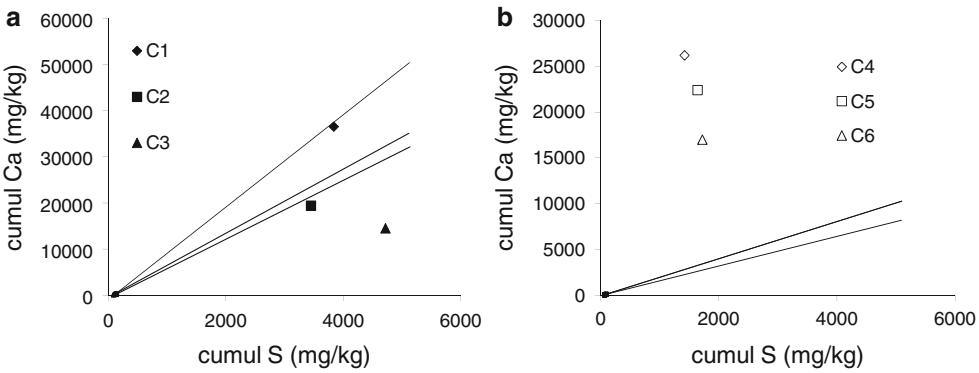

Fig. 9 Oxidation-neutralization curves extrapolation for fresh (**a**) and weathered (**b**) waste rocks

the fresh waste rocks in the present study, as plagioclase dissolution behavior changes with time (preferential Ca and Al dissolution in the early weathering stages). Nevertheless, one can assume that the weathered waste rocks response to kinetic tests are more representative of the long term behavior needed to assess the long-term AMD generation potential. Therefore, only the weathered waste rock results should be considered in the long term assessment of AMD generation of the Tio mine waste rocks, which suggests that the waste rocks are not acid-generating. Using the oxidation-neutralization curves involving only Ca as the neutralizing products takes into account only the plagioclase contribution to overall neutralization, and possibly the contribution of other minor Ca-bearing minerals. Not taking the pyroxene contribution in the overall neutralization is therefore conservative as pyroxenes are the second most important neutralizing minerals in the Tio mine waste rocks (see Table 3).

In addition to Ca released by the plagioclases in response to sulfide oxidation, the Mg, Al, and Si releases are also related to silicate dissolution. Therefore, all these elements could be considered as neutralization products in the oxidation-neutralization curve; the cumulative normalized loadings of Ca + Mg + Al + Si vs. S are shown on Fig. 8b, while the slopes and R^2 values are presented on Table 5. The comparison of the initial Ca + Mg + Al + Si values of the solid samples is not relevant, because Mg, Al, and Si are associated with other non-neutralizing minerals. However, it is interesting to note that the slopes of the fresh and weathered waste rocks Ca + Mg + Al + Si vs. S loadings are much more similar (between 7 and 14) than the slopes of only the Ca vs. S loadings (between 1 and 10). The similarities are explained by the fact that plagioclase in weathered waste rocks release more Si and Mg than the fresh ones, which release more Ca. Thus, the higher Mg and Si releases compensate for the lower Ca releases in weathered waste rocks and consequently, the slopes considering Ca + Mg + Si + Al are similar. Other studies obtained oxidation-neutralization curve slopes from fresh and weathered tailings that were similar to each other, where the neutralization was provided mainly by carbonates (Benzaazoua et al. 2004; Villeneuve 2004; Villeneuve et al. 2003, 2009).

These results have important implications for long-term extrapolations of humidity cell test results. First, it means that even though the main neutralizing minerals react differently after 25 years of natural weathering (regarding Ca, Mg, Al, and Si release), the response of the fresh waste rocks to humidity cell tests are very similar to those of the weathered waste rocks when considering all the elements related to silicate dissolution, including those implicated in secondary phase precipitation. Therefore, the hypotheses of the oxidation-neutralization curves are respected when silicate neutralization products (Ca, Mg, Al, and Si) are considered. This in turn implies that the precipitation of secondary Mg, Al, and Si minerals for the fresh and

weathered waste rocks do not affect the linearity of the oxidation-neutralization relation in the long term (at least for 25 years of weathering). Therefore, long-term extrapolation of humidity cell results can be done for the Tio mine waste rocks (and possibly for other waste rocks where neutralization is provided by plagioclase and pyroxenes), as was done by Benzaazoua et al. (2004) for mine tailings in which neutralization mainly came from carbonates. Even though the kinetic tests on the Tio mine waste rocks do not predict the onset of CND conditions as they occur in the field, the results show that long-term extrapolation of the kinetic tests results are acceptable when the hypotheses of the oxidation-neutralization curves are respected for 25 years of weathering.

Discussion

Since sulfides oxidize at similar rates in fresh and weathered Tio mine waste rocks (Table 4), the Ni release rates of fresh and weathered waste rocks should be of the same order. However, the Ni release rates of the weathered waste rocks are about an order of magnitude greater than those of the fresh waste rocks (Table 4) in humidity cell tests. The exact difference between fresh and weathered Ni release rates is difficult to establish because the Ni levels in leachates are regularly close to or below the detection limit, and therefore linear regressions of the cumulative Ni releases vs. time renders poor determination coefficients (R^2) in most of the humidity cell tests and for the fresh samples in weathering cells (Table 4). The relation between S and Ni releases are illustrated in Fig. 7d by comparing the S vs. Ni cumulative normalized loadings. The slopes of the cumulative normalized loadings of S vs. Ni of the fresh waste rocks tend to decrease and therefore to get closer to those of the weathered waste rocks with prolonged kinetic testing. Assuming that Ni is released from sulfide oxidation, two main hypotheses have to be considered in order to explain the Ni release rates differences between the fresh and altered waste rocks: (1) precipitation as secondary Ni phases and (2) Ni sorption within the waste rock materials.

Geochemical modeling using Vminteq (Online Supplementary Figure 1) show that no secondary Ni hydroxide ($Ni(OH)_{2(am)}$ and $Ni(OH)_{2(c)}$) is suspected to precipitate in the conditions of the kinetic tests. Geochemical simulations in JCHESS (Online Supplementary Figure 2) indicate that the secondary Ni silicate Ni_2SiO_4 species is suspected to precipitate at pH >8. The pH values measured in the humidity cell test leachates from the fresh waste rocks tended to decrease from 8.5 at the beginning to below 8 after 250 days, while in the case of the weathered waste rocks, the pH was rarely over 8 (Fig. 2). Moreover, the formation of secondary Ni minerals generally tend to be kinetically slow (Gunsinger et al. 2006, from Alpers et al. 1994 and Xue et al. 2001) and discrete minerals may be absent, even though they are thermodynamically stable. Therefore, secondary Ni minerals are most likely not responsible for the absence of Ni in the leachates of the kinetic tests in the present study.

Ni sorption is a phenomenon known to occur on Tio mine waste rock surfaces (Plante et al. 2010a). Many of the minerals found in the Tio mine waste rocks (ilmenite, plagioclase, chlorite, mica, spinel) show Ni sorption capacities (Plante et al. 2010a); plagioclase and ilmenite were demonstrated to be the main Ni sorption supports in the Tio mine waste rocks. Ni sorption is probably occurring on plagioclase surfaces via layered double hydroxides (LDH), as discussed earlier in the present paper. XPS measurements showed that the sorbed Ni was similar to $Ni(OH)_2$ on all these minerals (Biesinger et al. 2009; Plante et al. 2010a).

In addition to Ni sorption on primary minerals of the Tio mine waste rocks, some of the secondary minerals believed to form in the waste rocks are known to have Ni sorption capabilities. For example, kaolinite metal sorption is a well-documented phenomenon (e.g. Dadhich et al. 2003; Gu and Evans 2008; Gupta and Bhattacharyya 2008; Nachtegaal and Sparks 2003; Yavuz et al. 2003). Co (whose behavior is similar to Ni) uptake by kaolinite occurs in two stages (Thompson et al. 2000) during sorption experiments: a rapid initial uptake followed by slow uptake that continued even after thousands of hours, illustrating that equilibrium was difficult to achieve in the experiments. Consequently, these authors point out that equilibrium models probably offer only approximate simulation of kaolinite metal sorption and similar laboratory sorption systems, particularly when experiments are of much shorter duration. Ni uptake by kaolinite without reaching equilibrium within up to 7 months was also observed (Nachtegaal and Sparks 2003), revealing the formation of a Ni–Al LDH at the kaolinite surface resistant to mild desorption agents (0.02 M NaCl at pH6, 0.1 M $NaNO_3$ at pH 6, and HNO_3 at pH 4). Illite, a secondary mineral also believed to be present in the weathered Tio mine waste rocks, is also known as a Ni-sorbent material (e.g. Bradbury and Baeyens 2009; Cama et al. 2005; Echeverría et al. 2003; Gu and Evans 2007); Ni is retained on illite surfaces by precipitation of Ni–Al LDH (Elzinga and Sparks 2001), adsorbed as an outer-sphere complex (Elzinga and Sparks 2001) or inner-sphere complex (Echeverría et al. 2003). Therefore, illite must be considered as a potential Ni sink in the present kinetic test work. Ni sorption on weathered waste rock samples were shown not to reach equilibrium within 72 h, while equilibrium was attained on the fresh waste rocks; these behaviors may be

explained by the hypothesis that secondary minerals play a significant role in Ni sorption of the weathered Tio mine waste rocks.

Iron secondary minerals likely to precipitate in CND conditions (such as goethite, ferrihydrite or amorphous $Fe(OH)_3$, lepidocrocite, magnetite, and hematite; see Online Supplementary Figure 1) are known to play an important role in controlling the metal release in mine waters by sorption or co-precipitation (Alpers et al. 1994; Heikkinen and Räisänen 2008; Jambor and Blowes 1998). Also, both circumneutral pH and the presence of sulfates in drainage waters have been found to increase metal uptake by secondary iron oxyhydroxides phases (Heikkinen and Räisänen 2008; Swedlund and Webster 2001; Swedlund et al. 2003, 2009). Sequential extractions on naturally weathered Tio mine waste rocks and post-kinetic test samples show that a significant portion of Ni is associated with reducible phases, mainly composed of iron oxyhydroxides (Plante et al. 2010a) SEM observations on polished sections of the Tio mine waste rocks show abundant iron oxyhydroxides phases, particularly around weathered iron sulfide particles (Pepin 2009; Plante 2010).

The fact that the weathered samples release more Ni vs S than the fresh ones (Fig. 7d) suggest that their Ni uptake has reached a level close to its maximum uptake capacity, leaving more Ni in solution than in fresh waste rocks, and/or that secondary Si and Al mineral precipitation and their subsequent Ni uptake is less significant in weathered waste rocks than fresh waste rocks, as suggested by geochemical simulations (Online Supplementary Figures 1, 2). Both these hypotheses are consistent with the general observation that weathered waste rocks release more Ni than fresh ones.

Some of the Tio mine waste rocks piles generate Ni-contaminated neutral drainage in the field that may exceed the regulated levels. However, the humidity cell leachates show Ni concentrations way below the regulated levels, even for weathered waste rock samples. Consequently, humidity cell tests on the Tio mine waste rocks do not adequately predict the Ni levels that are observed on field test pads and in actual waste rock piles at the mine site (Bussière et al. 2008; Pepin 2009; Plante 2010;). These results highlight the difficulty of extrapolating humidity cell results to the field scale for CND-generating mine waste. Only taking humidity cell tests into account in the drainage quality prediction of the Tio mine waste rocks, without separate sorption studies and field observations and investigations, would have generated a false safe assessment for drainage quality at the Tio mine site. However, humidity cell tests do evaluate the waste rock geochemical behavior, which is critical in understanding the development of CND conditions at the field scale.

Conclusion

The main conclusions that can be drawn from this study are:

- The acid-neutralization capacities of the Tio mine waste rocks are provided mostly by plagioclase and pyroxene minerals in the waste rocks;
- Secondary minerals are ubiquitous in the weathered waste rocks and control the mobility of Al, Mg, and Si in drainage waters;
- Even though the main neutralizing minerals react differently after 25 years of natural weathering (regarding Ca, Mg, Al, and Si release), the response of the fresh waste rocks during humidity cell leaching are very similar to those of the weathered waste rocks when considering all the elements related to silicate dissolution, including those implicated in secondary phase precipitation;
- The long-term extrapolation of kinetic cell results to the long term can be done for the Tio mine waste rocks (and possibly for other waste rocks whose neutralization is provided by the neutralizing silicates plagioclase and pyroxenes), as was done by Benzaazoua et al. (2004) for mine tailings in which neutralization mainly came from carbonates;
- The Tio mine waste rocks would not be not acid generating in the long term, as determined by humidity cells on fresh and weathered waste rocks interpreted by conservative oxidation-neutralization curves;
- Even though sulfide oxidation occurs at similar rates in fresh and weathered waste rocks, Ni generation is greater in weathered waste rocks, as Ni sorption capacities of the weathered waste rocks are approaching saturation.

These results highlight the fact that metal mobility in near-neutral drainage is often driven by sorption phenomena that are not straightforward. Although humidity cells implicitly account for sorption phenomena in the overall geochemistry of the system, the present study demonstrates that separate sorption studies are needed to adequately interpret the humidity cell results for the Tio mine waste rocks. The present study also highlights the limits of humidity cell tests in predicting field-scale metal loadings: the Ni levels remain well below the observed levels on the field. More insight is needed in order to extrapolate lab results to the field scale.

Acknowledgments The authors thank the NSERC Polytechnique-UQAT Chair in Environment and Mine Wastes Management and the NSERC Collaborative Research and Development Grants for funding this project. The authors also thank Donald Laflamme of Rio Tinto, Iron and Titanium, Inc., for the funding and constant support of this

project, as well as Genevieve Pepin for providing samples and insight. Alain Perreault, Mélanie Bélanger, and Mathieu Villeneuve of URSTM, UQAT are also acknowledged for their laboratory support.

References

Alpers CN, Nordstrom DK (1999) Geochemical modeling of water-rock interactions in mining environments. In: Plumlee GS, Logsdon MJ (eds) Environmental Geochemistry of Mineral Deposits, Reviews in Economic Geology, vol 6A. Soc Econ Geol, Littleton, CO, USA, pp 289–324

Alpers CN, Blowes DW, Nordstrom DK, Jambor JL (1994) Secondary minerals and acid mine-water chemistry. In: Blowes DW, Jambor JL (eds) The Environmental Geochemistry of Sulfide Mine-wastes, Mineralogical Assoc of Canada, Short Course Handbook, vol 22. Ottawa, Canada, pp 246–270

ASTM Standard D5744-07 (2001) Standard Test method for laboratory weathering of solid materials using a humidity cell. ASTM International. doi:10.1520/D5744-07. Accessible at: www.astm.org

Aubertin M, Bussière B, Bernier L (2002) Environnement et gestion des résidus miniers. Manuel sur Cédérom. Les Presse Internationales Polytechnique, Montréal, Canada

Benzaazoua M, Bussière B, Dagenais AM, Archambault M (2004) Kinetic tests comparison and interpretation for prediction of the Joutel tailings acid generation potential. Environ Geol 46:1086–1101

Biesinger MC, Payne BP, Lau LWM, Gerson A, Smart RSC (2009) X-ray photoelectron spectroscopic chemical state quantification of mixed nickel metal, oxide and hydroxide systems. Surf Interface Anal 41:324–332

Blake RE, Walter LM (1999) Kinetics of feldspar and quartz dissolution at 70–80°C and near-neutral pH: effects of organic acids and NaCl. Geochim Cosmochim Acta 63(13–14): 2043–2059

Blowes DW, Ptacek CJ, Jambor JL, Weisener CG (2003) The geochemistry of acid mine drainage. In: Holland HD, Turekian KK (eds) Treatise on geochemistry, Ch 9.05. Pergamon, Oxford, pp 149–204, ISBN: 978-0-08-043751-4

Blum AE, Stillings LL (1995) Feldspar dissolution kinetics. Rev Mineral Geochem 31:291–351

Bradbury MH, Baeyens B (2009) Sorption modelling on illite Part I: Titration measurements and the sorption of Ni, Co, Eu and Sn. Geochim Cosmochim Acta 73:990–1003

Brantley SL, Heinrich DH, Karl KT (2003) Reaction kinetics of primary rock-forming minerals under ambient conditions. In: Holland HD, Turekian KK (eds) Treatise on geochemistry, Ch. 5.03. Pergamon, Oxford, pp 73–117, ISBN: 978-0-08-043751-4

Brunauer S, Emmett PH, Teller E (1938) Adsorption of gases in multimolecular layers. J Am Chem Soc 60:309–319

Bussière B (2007) Colloquium 2004: hydrogeotechnical properties of hard rock tailings from metal mines and emerging geoenvironmental disposal approaches. Can Geotech J 44:1019–1052

Bussiere B, Benzaazoua M, Aubertin M, Mbonimpa M (2004) A laboratory study of covers made of low-sulphide tailings to prevent acid mine drainage. Environ Geol 45:609–622

Bussiere B, Dagenais AM, Villeneuve M, Plante B (2005) Caractérisation environnementale d'un échantillon de stériles de la mine Tio. Technical report. Unité de recherche et de service en technologie minérale, Rouyn-Noranda, Canada

Bussière B, Benzaazoua M, Plante B, Pepin G, Aubertin M, Laflamme D (2008) Évaluation du comportement géochimique des stériles de la mine Tio, Havre-Saint-Pierre, Québec. Proc, Symp 2008 sur l'Environnement et les mines. Rouyn-Noranda, Canada, CD-ROM

Cama J, Metz V, Ganor J (2002) The effect of pH and temperature on kaolinite dissolution rate under acidic conditions. Geochim Cosmochim Acta 66:3913–3926

Cama J, Ayora C, Querol X, Moreno N (2005) Metal adsorption on clays from pyrite contaminated soil. J Environ Eng 131: 1052–1056

Carroll SA, Knauss KG (2005) Dependence of labradorite dissolution kinetics on CO2(aq), Al(aq), and temperature. Chem Geol 217: 213–225

Casey WH, Westrich HR, Massis T, Banfield JF, Arnold GW (1989) The surface of labradorite feldspar after acid hydrolysis. Chem Geol 78:205–218

Cruz R, Mendez BA, Monroy M, Gonzalez I (2001) Cyclic voltammetry applied to evaluate reactivity in sulfide mining residues. Appl Geochem 16:1631–1640

Dadhich AS, Beebi SK, Kavitha GV, Chaitanya KVK (2003) Adsorption kinetics of Ni(II) using Kaolinite clay part-I. Asian J Chem 15:772–780

D'Espinose De La Caillerie JB, Kermarec M, Clause O (1995) Impregnation of ?-alumina with Ni(II) or Co(II) ions at neutral pH: Hydrotalcite-type coprecipitate formation and characterization. J Am Chem Soc 117:11471–11481

Echeverría J, Indurain J, Churio E, Garrido J (2003) Simultaneous effect of pH, temperature, ionic strength, and initial concentration on the retention of Ni on illite. Colloids Surf A 218: 175–187

Eick MJ, Naprstek BR, Brady PV (2001) Kinetics of Ni(II) sorption and desorption on kaolinite: Residence time effects. Soil Sci 166:11–17

Elzinga EJ, Sparks DL (2001) Reaction condition effects on nickel sorption mechanisms in illite-water suspensions. Soil Sci Soc Am J 65:94–101

Felmy AR, Griven JB, Jenne EA (1984) MINTEQ: a computer program for calculating aqueous geochemical equilibria. NTIS. Springfield, VA, USA

Ford RG, Scheinost AC, Scheckel KG, Sparks DL (1999) The link between clay mineral weathering and the stabilization of Ni surface precipitates. Environ Sci Technol 33:3140–3144

Frost MT, Grey IE, Harrowfield IR, Mason K (1983) The dependence of alumina and silica contents on the extent of alteration of weathered ilmenites from Western Australia. Mineral Mag 47:201–208

Grey IE, Reid AF (1975) The structure of pseudorutile and its role in the natural alteration of pseudorutile. Am Mineral 60: 898–906

Grey I, MacRae C, Silvester E, Susini J (2005) Behaviour of impurity elements during the weathering of ilmenite. Mineral Mag 69:437–446

Gu X, Evans LJ (2007) Modelling the adsorption of Cd(II), Cu(II), Ni(II), Pb(II), and Zn(II) onto Fithian illite. J Coll Interf Sci 307:317–325

Gu X, Evans LJ (2008) Surface complexation modelling of Cd(II), Cu(II), Ni(II), Pb(II) and Zn(II) adsorption onto kaolinite. Geochim Cosmochim Acta 72:267–276

Gunsinger MR, Ptacek CJ, Blowes DW, Jambor JL, Moncur MC (2006) Mechanisms controlling acid neutralization and metal mobility within a Ni-rich tailings impoundment. Appl Geochem 21:1301–1321

Gupta SS, Bhattacharyya KG (2008) Immobilization of Pb(II), Cd(II) and Ni(II) ions on kaolinite and montmorillonite surfaces from aqueous medium. J Environ Manage 87:46–58

Hakkou R, Benzaazoua M, Bussière B (2008) Acid mine drainage at the abandoned kettara mine (Morocco): 2. mine waste geochemical behavior. Mine Water Environ 27:160–170

Heikkinen PM, Räisänen ML (2008) Mineralogical and geochemical alteration of Hitura sulphide mine tailings with emphasis on nickel mobility and retention. J Geochem Explor 97:1–20

Heikkinen P, Räisänen M, Johnson R (2009) Geochemical characterization of seepage and drainage water quality from two sulphide mine tailings impoundments: acid mine drainage vs. neutral mine drainage. Mine Water Environ 28:30–49

Hellmann R, Penisson JM, Hervig RL, Thomassin JH, Abrioux MF (2003) An EFTEM/HRTEM high-resolution study of the near surface of labradorite feldspar altered at acid pH: evidence for interfacial dissolution-reprecipitation. Phys Chem Miner 30: 192–197

Hodgkinson J, Cox ME, McLoughlin S (2008) Coupling mineral analysis with conceptual groundwater flow modelling: the source and fate of iron, aluminium and manganese in a back-barrier island. Chem Geol 251:77–98

Holmström H, Salmon UJ, Carlsson E, Petrov P, Öhlander B (2001) Geochemical investigations of sulfide-bearing tailings at Kristineberg, northern Sweden, a few years after remediation. Sci Total Environ 273:111–133

Inskeep WP, Nater EA, Bloom PR, Vandervoort DS, Erich MS (1991) Characterization of laboratory weathered labradorite surfaces using X-ray photoelectron spectroscopy and transmission electron microscopy. Geochim Cosmochim Acta 55:787–800

Jambor JL, Blowes DW (1998) Theory and applications of mineralogy in environmental studies of sulfide-bearing mine wastes. In: Cabri LJ, Vaughan DJ (eds) Modern Approaches to Ore and Environmental Mineralogy. Short Course Series vol 27. Mineralogical Assoc of Canada, Ottawa, Canada, pp 367–401

Jambor JL, Dutrizac JE, Groat LA, Raudsepp M (2002) Static tests of neutralization potentials of silicate and aluminosilicate minerals. Environ Geol 43(1–2):1–17

Jambor JL, Dutrizac JE, Raudsepp M (2007) Measured and computed neutralization potentials from static tests of diverse rock types. Environ Geol 52:1019–1031

Janßen A, Golla-Schindler U, Putnis A (2008) The mechanism of ilmenite leaching during experimental alteration in HCl-solution. Proc, EMC 14th European Microscopy Congress. Aachen, Germany, pp 825–826

Johnson RH, Blowes DW, Robertson WD, Jambor JL (2000) The hydrogeochemistry of the Nickel Rim mine tailings impoundment, Sudbury, Ontario. J Contam Hydrol 41:49–80

KWONG YTJ (1993) Prediction and prevention of acid rock drainage from a geological and mineralogical perspective. MEND report 1.32.1 CANMET, Ottawa, 47 pp

Lawrence RW, Scheske M (1997) A method to calculate the neutralization potential of mining wastes. Environ Geol 32: 100–106

Lawrence RW, Wang Y (1997) Determination of neutralization potential in the prediction of acid rock drainage. Proc, 4th International Conf on Acid Rock Drainage (ICARD). Vancouver, Canada, pp 451–464

Lener EF (1997) Mineral chemistry of heavy minerals in the Old Hickory Deposit, Sussex and Dinwiddie Counties, Virginia. PhD Thesis, Virginia Polytechnic Institute and State University, Blacksburg, USA

Li MG (2000) Acid rock drainage prediction for low-sulfide, low-neutralization potential mine wastes. Proc, 5th ICARD. Denver, CO, USA, pp 567–580

McGregor RG, Blowes DW, Jambor JL, Robertson WD (1998) Mobilization and attenuation of heavy metals within a nickel mine tailings impoundment near Sudbury, Ontario, Canada. Environ Geol 36:305–319

MEND (1991) Acid Rock Drainage Prediction Manual. MEND Project 1.16.1b, report by Coastech Research. MEND. Natural Resources Canada, Ottawa, Canada

Mücke A, Bhadra Chaudhuri JN (1991) The continuous alteration of ilmenite through pseudorutile to leucoxene. Ore Geol Revi 6:25–44

Muir IJ, Nesbitt HW (1992) Controls on differential leaching of calcium and aluminum from labradorite in dilute electrolyte solutions. Geochim Cosmochim Acta 56:3979–3985

Muir IJ, Nesbitt HW (1997) Reactions of aqueous anions and cations at the labradorite-water interface: coupled effects of surface processes and diffusion. Geochim Cosmochim Acta 61: 265–274

Muir IJ, Bancroft MG, Nesbitt WH (1989) Characteristics of altered labradorite surfaces by SIMS and XPS. Geochim Cosmochim Acta 53:1235–1241

Muir IJ, Bancroft MG, Shotyk W, Nesbitt WH (1990a) A SIMS and XPS study of dissolving plagioclase. Geochim Cosmochim Acta 54:2247–2256

Muir IJ, Bancroft GM, Nesbitt HW (1990b) Analysis of dissolved plagioclase mineral surfaces. Surf Interface Anal 16:581–582

Nachtegaal M, Sparks DL (2003) Nickel sequestration in a kaolinite-humic acid complex. Environ Sci Technol 37:529–534

Nair AG, Suresh Babu DS, Vivekanandan KL, Vlach SRF (2006) Differential alteration of ilmenite in a tropical beach placer, southern India: microscopic and electron probe evidences. Resour Geol 56:75–81

Nair AG, Suresh Babu DS, Damodaran KT, Shankar R, Prabhu CN (2009) Weathering of ilmenite from Chavara deposit and its comparison with Manavalakurichi placer ilmenite, southwestern India. J Asian Earth Sci 34:115–122

Nicholson RV (2004) Overview of near neutral pH drainage and its mitigation: results of a MEND study. MEND Ontario workshop, Sudbury, Canada

Nugent MA, Brantley SL, Pantano CG, Maurice PA (1998) The influence of natural mineral coatings on feldspar weathering. Nature 395:588–591

Oberlin A, Couty R (1970) Conditions of kaolinite formation during alteration of some silicates by water at 200 Â°C. Clays Clay Miner 18(6):347–356

Oelkers EH, Schott J (2001) An experimental study of enstatite dissolution rates as a function of pH, temperature, and aqueous Mg and Si concentration, and the mechanism of pyroxene/pyroxenoid dissolution. Geochim Cosmochim Acta 65:1219–1231

Oelkers EH, Golubev SV, Chairat C, Pokrovsky OS, Schott J (2009) The surface chemistry of multi-oxide silicates. Geochim Cosmochim Acta 73(16):4617–4634

Paktunc AD (1999a) Characterization of mine wastes for prediction of acid mine drainage. In: Azcue JM (ed) Environmental Impacts of Mining Activities. Emphasis on Mitigation and Remedial Measures, Springer-Verlag, Berlin, Germany, pp 19–40

Paktunc AD (1999b) Mineralogical constraints on the determination of neutralization potential and prediction of acid mine drainage. Environ Geol 39:103–112

Peltier E, Allada R, Navrotsky A, Sparks DL (2006) Nickel solubility and precipitation in soils: a thermodynamic study. Clays Clay Miner 54:153–164

Pepin G (2009) Évaluation du comportement géochimique de stériles potentiellement générateurs de drainage neutre contaminé à l'aide de cellules expérimentales in situ. Master's thesis, Dépt des génies civil, géologique et des mines, École Polytechnique de Montréal, Montreal, Canada

Pepin G, Bussière B, Aubertin M, Benzaazoua M, Plante B, Laflamme D, Zagury GJ (2008) Field experimental cells to evaluate the generation of contaminated neutral drainage by waste rocks at the Tio mine, Quebec, Canada. Proc, 10th International Mine Water Assoc Congress on Mine Water and the Environment, Czech Republic, pp 309–312

Pettit CM, Scharer JM, Chambers DB, Halbert BE, Kirkaldy JL, Bolduc L (1999) Neutral mine drainage. Proceedings, Sudbury Mining and the Environment International Conference, vol 2, pp 829–838

Plante B (2005) Comparaison des essais statiques et évaluation de l'effet de l'altération pour des rejets de concentrateur à faible potentiel de génération d'acide. In Dépt des génies civil. géologique et des mines. École Polytechnique de Montréal, Montréal, Canada

Plante B (2010) Prédiction du drainage neutre contaminé en Ni: cas de la mine Tio. PhD thesis, UQAT, Québec

Plante B, Benzaazoua M, Bussière B, Pepin G, Laflamme D (2008) Geochemical behaviour of nickel contained in Tio mine waste rocks. In: Rapantova N, Hrkal Z (eds) Proceedings, 10th IMWA Congress on Mine Water and the Environment, Czech Republic, p 317–320

Plante B, Benzaazoua M, Bussière B, Biesinger MC, Pratt AR (2010a) Study of Ni sorption onto Tio mine waste rock surfaces. Submitted to applied geochemistry

Plante B, Benzaazoua M, Bussière B (2010b) Contaminated neutral drainage prediction: kinetic testing and sorption studies by modified weathering cells. In preparation

Price WA, Kwong YTJ (1997) Waste rock weathering, sampling and analysis: observations from the British Columbia Ministry of Employment and Investment Database. Proc, 4th ICARD. Vancouver, Canada, pp 31–45

Price WA, Morin K, Hutt N (1997) Guidelines for the prediction of acid rock drainage and metal leaching for mines in British Columbia: Part II. Recommended procedures for static and kinetic testing. Proc, 4th ICARD, Vancouver, Canada

QIT (2005) Preparing a sustainable future—Social and environmental report 2005. Available at: http://www.qit.com/pdf/QIT_BulSocEnv05_ANG.pdf

Rietveld HM (1993) The Rietveld Method. Oxford University Press, Oxford, UK

Roberts DR, Scheidegger AM, Sparks DL (1999) Kinetics of mixed NI-AL precipitate formation on a soil clay fraction. Environ Sci Technol 33:3749–3754

Sapsford DJ, Bowell RJ, Dey M, Williams KP (2009) Humidity cell tests for the prediction of acid rock drainage. Min Eng 22: 25–36

Scharer JM, Garg V, Smith R, Halbert BE (1991) Use of steady state models for assessing acid generation in pyritic mine tailings. Proceedings, 2nd ICARD, Montréal. CANMET, Ottawa, Vol 2, pp 211–229

Scharer JM, Nicholson RV, Halbert B, Snodgrass WJ (1994) A computer program to assess acid generation in pyrite tailings. In: Alpers CN, Blowes DW (eds) Environmental Geochemistry of Sulfide Oxidation, vol 550. Am Chem Soc Symp Series, Washington DC, USA, pp 135–152

Scheckel KG, Sparks DL (2001) Division S-2—Soil chemistry: dissolution kinetics of nickel surface precipitates on clay mineral and oxide surfaces. Soil Sci Soc Am J 65:685–694

Scheckel KG, Scheinost AC, Ford RG, Sparks DL (2000) Stability of layered Ni hydroxide surface precipitates–a dissolution kinetics study. Geochim Cosmochim Acta 64:2727–2735

Scheidegger AM, Lamble GM, Sparks DL (1997) Spectroscopic evidence for the formation of mixed-cation hydroxide phases upon metal sorption on clays and aluminum oxides. J Coll Interf Sci 186:118–128

Scheidegger AM, Strawn DG, Lamble GM, Sparks DL (1998) The kinetics of mixed Ni-Al hydroxide formation on clay and aluminum oxide minerals: a time-resolved XAFS study. Geochim Cosmochim Acta 62:2233–2245

Scheinost AC, Sparks DL (2000) Formation of layered single- and double-metal hydroxide precipitates at the mineral/water interface: a multiple-scattering XAFS analysis. J Coll Interf Sci 223:167–178

Scheinost AC, Ford RG, Sparks DL (1999) The role of Al in the formation of secondary Ni precipitates on pyrophyllite, gibbsite, talc, and amorphous silica: a DRS study. Geochim Cosmochim Acta 63:3193–3203

Schott J, Berner RA, Sjöberg EL (1981) Mechanism of pyroxene and amphibole weathering–I. experimental studies of iron-free minerals. Geochim Cosmochim Acta 45:2123–2135

Schroeder PA, Le Golvan JJ, Roden MF (2002) Weathering of ilmenite from granite and chlorite schist in the Georgia Piedmont. Am Mineral 87:1616–1625

Schweda P, Sjöberg L, Södervall U (1997) Near-surface composition of acid-leached labradorite investigated by SIMS. Geochim Cosmochim Acta 61:1985–1994

Sobek AA, Schuller WA, Freeman JR, Smith RM (1978) Field and laboratory methods applicable to overburdens and minesoils. EPA-600/2–78-054. US Environmental Protection Agency, Washington DC, USA, pp 47–50

Sparks DL (2001) Elucidating the fundamental chemistry of soils: past and recent achievements and future frontiers. Geoderma 100:303–319

SRK (1989) Draft Acid Rock Drainage Technical Guide. BCAMD Task Force, Vancouver, Canada

Stefánsson A (2001) Dissolution of primary minerals of basalt in natural waters: I. Calculation of mineral solubilities from 0°C to 350°C. Chem Geol 172:225–250

Swedlund PJ, Webster JG (2001) Cu and Zn ternary surface complex formation with SO4 on ferrihydrite and schwertmannite. Appl Geochem 16:503–511

Swedlund PJ, Webster JG, Miskelly GM (2003) The effect of SO4 on the ferrihydrite adsorption of Co, Pb and Cd: ternary complexes and site heterogeneity. Appl Geochem 18:1671–1689

Swedlund PJ, Webster JG, Miskelly GM (2009) Goethite adsorption of Cu(II), Pb(II), Cd(II), and Zn(II) in the presence of sulfate: properties of the ternary complex. Geochim Cosmochim Acta 73:1548–1562

Thompson HA, Parks GA, Brown GE (2000) Formation and release of cobalt(II) sorption and precipitation products in aging kaolinite-water slurries. J Colloid Interface Sci 222:241–253

USEPA (1999) MINTEQA2, Metal speciation equilibrium model for surface and ground water, version 4.0. http://epa.gov/ceampubl/mmedia/minteq/index.html

van der Lee J, De Windt L (2002) CHESS Tutorial and cookbook: updated for version 3.0. Users manual Nr. LHM/RD/02/13. École des Mines de Paris, Fontainebleau, France

Villeneuve M (2004) Évaluation du comportement géochimique à long terme de rejets miniers à faible potentiel de génération d'acide à l'aide d'essais cinétiques. Dépt des génies civil. géologique et des mines. École Polytechnique de Montréal, Montréal, Canada

Villeneuve M, Bussière B, Benzaazoua M, Aubertin M, Monroy M (2003) The influence of kinetic test type on the geochemical response of low acid generating potential tailings. Proc, Tailings and Mine Waste '03, Sweets and Zeitlinger. Vail, CO., USA, pp 269–279

Villeneuve M, Bussière B, Benzaazoua M (2009) Assessment of interpretation methods for kinetic tests performed on tailings having a low acid generating potential. Proceedings, Securing the Future and 8th ICARD, Skelleftea, Sweden

White AF, Peterson ML (1996) Reduction of aqueous transition metal species on the surfaces of Fe(II) -containing oxides. Geochim Cosmochim Acta 60:3799–3814

White AF, Peterson ML, Hochella MF Jr (1994) Electrochemistry and dissolution kinetics of magnetite and ilmenite. Geochim Cosmochim Acta 58:1859–1875

White WW III, Lapakko KA, Cox RL (1999) Static-test methods most commonly used to predict acid-mine drainage: practical guidelines for use and interpretation. In: Plumlee GS, Logsdon MJ (eds), The environmental geochemistry of mineral deposits: Part A. Processes, techniques, and health issues, vol 6A, pp 325–338, Rev Econ Geol

Wilson MJ (2004) Weathering of the primary rock-forming minerals: processes, products and rates. Clay Min 39(3):233–266

Wolery T (1992) EQ3/6: A software package for geochemical modelling of aqueous systems: package overview and installation guide. Technical Report UCRL-MA-110662 pt I, Lawrence Livermore National Lab. Livermore, CA, USA

Xiao Y, Lasaga AC (1994) Ab initio quantum mechanical studies of the kinetics and mechanisms of silicate dissolution: $H^+(H_3O^+)$ catalysis. Geochim Cosmochim Acta 58:5379–5400

Xue HB, Jansen S, Prasch A, Sigg L (2001) Nickel speciation and complexation kinetics freshwater by ligand exchange and DPCSV. Environ Sci Technol 35(3):539–546

Yamaguchi NU, Scheinost AC, Sparks DL (2002) Influence of gibbsite surface area and citrate on Ni sorption mechanisms at pH 7.5. Clays Clay Miner 50:784–790

Yavuz Ö, Altunkaynak Y, Güzel F (2003) Removal of copper, nickel, cobalt and manganese from aqueous solution by kaolinite. Water Res 37:948–952

Zakaznova-Herzog VP, Nesbitt HW, Bancroft GM, Tse JS (2008) Characterization of leached layers on olivine and pyroxenes using high-resolution XPS and density functional calculations. Geochim Cosmochim Acta 72(1):69–86

Zhang L, Lüttge A (2009) Morphological evolution of dissolving feldspar particles with anisotropic surface kinetics and implications for dissolution rate normalization and grain size dependence: a kinetic modeling study. Geochim Cosmochim Acta 73:6757–6770